Converting Quasiclassical States into Arbitrary Fock State Superpositions in a Superconducting Circuit

W. Wang,[1] L. Hu,[1] Y. Xu,[1] K. Liu,[1] Y. Ma,[1] Shi-Biao Zheng,[2,*] R. Vijay,[3] Y. P. Song,[1] L.-M. Duan,[1,4,†] and L. Sun[1,‡]
[1]*Center for Quantum Information, Institute for Interdisciplinary Information Sciences, Tsinghua University, Beijing 100084, China*
[2]*Fujian Key Laboratory of Quantum Information and Quantum Optics, College of Physics and Information Engineering, Fuzhou University, Fuzhou, Fujian 350116, China*
[3]*Department of Condensed Matter Physics and Materials Science, Tata Institute of Fundamental Research, Homi Bhabha Road, Mumbai 400005, India*
[4]*Department of Physics, University of Michigan, Ann Arbor, Michigan 48109, USA*
(Received 8 September 2016; published 1 June 2017)

We propose and experimentally demonstrate a new method to generate arbitrary Fock state superpositions in a superconducting quantum circuit, where a qubit is dispersively coupled to a microwave cavity mode. Here, the qubit is used to conditionally modulate the probability amplitudes of the Fock state components of a coherent state to those of the desired superposition state, instead of pumping photons one by one into the cavity as in previous schemes. Our method does not require the adjustment of the qubit frequency during the cavity state preparation and is more robust to noise and accumulation of experimental errors compared to previous ones. Using the method, we experimentally generate phase eigenstates under various Hilbert-space dimensions and squeezed states, which are useful for the quantum walk and high-precision measurement.

DOI: 10.1103/PhysRevLett.118.223604

The creation and manipulation of nonclassical states of a harmonic oscillator (e.g., a light field) are important subjects in quantum optics [1]. Among these states, Fock states and their controlled superpositions are particularly appealing. Fock states are eigenstates of the oscillator Hamiltonian with definite numbers of energy quanta. When the quantum number is nonzero, such states show a negative quasiprobability distribution in certain regimes of the phase space, which represents an inherent nonclassical feature [2]. Because of the energy dissipation, Fock states decay at a rate linearly scaling with the quantum number, and as a result, these states play a central role for the exploration of environment-induced decoherence [3,4] and serve as a good example for the demonstration of quantum feedback operations [5,6]. Superposing different Fock states will give rise to new nonclassical features due to their quantum interference, e.g., the reduction of the fluctuation in one quadrature below the vacuum level (squeezing) [7], which would enable high-precision measurement [8]. Recently, it has been shown that superpositions of Fock states with binomial coefficients are useful for quantum error correction [9]. As such, controlled generation of Fock states and their superpositions is interesting both for foundational tests of quantum theory and for practical applications.

Previous methods employed a step-by-step algorithm [10,11], where in each step, the quantum state of a two-level system is manipulated in a controllable manner and then transferred to the harmonic oscillator, increasing the quantum number of the largest Fock state component in the superposition by one. After N steps, the oscillator evolves from the ground state to any superposition of the first $N+1$ number states. Such a technique was first demonstrated on the harmonic motion of a trapped ion [12] and then implemented in a superconducting resonator [13,14], using a qubit with fast frequency tunability to coherently pump photons from external microwave drive pulses into the resonator. More recently, it was shown that $2N$ selective number-dependent arbitrary phase gates, together with $2N+1$ displacement operations, can be used to construct such superposition states [15]. Following this proposal, a one-photon Fock state was created in a circuit QED system [16]. With a similar setup, the gradient ascent pulse engineering method [17,18] was recently used for creating the six-photon state and four-component cat states [19]. In the context of cavity QED, Fock states and cat states of a cavity were conditionally generated with Rydberg atoms dispersively coupled to the cavity mode [2].

Here, we propose and experimentally demonstrate a distinct method to synthesize any superposition of Fock states for the field stored in a cavity that is dispersively coupled to a qubit. Our method relies on photon-number-dependent qubit rotations, which allow for individually manipulating the probability amplitudes of the Fock state components of a coherent state. Coherent states are quasiclassical states characterized by a complex amplitude [2] and can be generated by using a classical drive. The photon-number-dependent shift in the qubit frequency, arising from the dispersive qubit-cavity coupling, enables one to use carefully tailored microwave drive signals to individually control the qubit transition amplitude associated with each Fock state. The subsequent measurement of the qubit transition conditionally projects the cavity to a superposition

of Fock states, with the probability amplitude of each state component being proportional to the associated qubit transition amplitude, controllable by the amplitude and phase of the corresponding drive signal. Furthermore, during the preparation process, the qubit-cavity detuning needs not to be adjusted, which is important for quantum state engineering in circuit QED systems with three-dimensional cavities [16,20–22], where it is difficult to adjust the qubit frequency. We implement the experiment in a superconducting circuit, where a cavity is coupled to a transmon qubit. We analyze the produced states by measuring the Wigner functions, showing good agreement with the desired ones.

The system under investigation consists of a qubit dispersively coupled to a cavity and driven by a classical microwave containing $N+1$ frequency components. In the interaction picture, the Hamiltonian for the total system is

$$H_I = -\chi_{\rm qc} a^\dagger a |e\rangle\langle e| + \left(\sum_{n=0}^{N} \Omega_n e^{i(\delta_n t+\phi_n)} |e\rangle\langle g| + \text{H.c.}\right), \tag{1}$$

where $|e\rangle$ and $|g\rangle$ denote the excited and ground states of the qubit, $a^\dagger$ and a are the creation and annihilation operators of the photonic field in the cavity, $\chi_{\rm qc}$ is the qubit's frequency shift induced by per photon in the cavity due to the dispersive qubit-cavity coupling, δ_n is the detuning between the qubit and the nth driving component with a Rabi frequency Ω_n and a phase ϕ_n, and H.c. denotes the Hermitian conjugate. The qubit is initially in the ground state $|g\rangle$ and the cavity in a coherent state

$$|\alpha\rangle = \sum_{n=0}^{\infty} c_n |n\rangle, \tag{2}$$

where $c_n = \exp(-|\alpha|^2/2)\alpha^n/\sqrt{n!}$ is the probability amplitude for having n photons. The photon-number-dependent shift of the qubit transition frequency enables one to individually modulate the probability amplitudes of the superposed Fock states in $|\alpha\rangle$ with a carefully tailored microwave drive addressing the qubit. Our aim is to convert such a quasiclassical state to a target quantum state

$$|\psi_d\rangle = \sum_{n=0}^{N} d_n |n\rangle, \tag{3}$$

with the desired complex amplitudes d_n for the corresponding Fock state components.

Under the condition $\delta_n = n\chi_{\rm qc}$ and $\Omega_n \ll \chi_{\rm qc}$, the nth component resonantly drives the qubit transition when the cavity is in the Fock state $|n\rangle$ but does not affect the qubit state if the cavity is in any other Fock state due to large detunings. The dynamics governed by H_I enables one to individually control the transition in each subspace $\{|g,n\rangle, |e,n\rangle\}$ (the notation denotes $|qubit, cavity\rangle$); there is no interaction between different subspaces. After an interaction time τ, the qubit-cavity system evolves to

$$|\psi_{\rm qc}(\tau)\rangle = \sum_{n=0}^{\infty} c_n [\cos\beta_n |g,n\rangle - i e^{i(\phi_n + n\chi_{\rm qc}\tau)} \sin\beta_n |e,n\rangle], \tag{4}$$

where $\beta_n = \int_0^\tau \Omega_n dt$ is the pulse area associated with the nth frequency component. We take $\beta_n = 0$ for $n > N$, where N is the maximum photon number in the desired target state. The detection of the qubit in the state $|e\rangle$ projects the cavity to the superposition state

$$|\psi_c\rangle = \mathcal{N} \sum_{n=0}^{N} c_n e^{i(\phi_n + n\chi_{\rm qc}\tau)} \sin\beta_n |n\rangle, \tag{5}$$

where $\mathcal{N} = [\sum_{n=0}^{N} |c_n|^2 \sin^2\beta_n]^{-1/2}$ is a normalization factor. The final cavity state $|\psi_c\rangle$ is equivalent to the desired state $|\psi_d\rangle$ when the parameters β_n and ϕ_n are appropriately chosen so that $d_n = \mathcal{N} c_n \sin\beta_n e^{i(n\chi_{\rm qc}\tau+\phi_n)}$. To maximize the success probability $P = 1/\mathcal{N}^2$, we numerically optimize the parameters $|\alpha|$ and β_n, with the optimal values depending upon the desired state.

Compared with the previous method [11], our protocol has the advantage of having no need to tune the qubit frequency but has the disadvantage that the desired states are created conditionally, with the success probability scaling in different ways for different types of states. To illustrate the state-dependent efficiency scaling, in Fig. 1, we display the optimal success probability as functions of N for the Fock state $|N\rangle$ (black), two-component superposition $(|0\rangle + |N\rangle)/\sqrt{2}$ (blue), and truncated phase state (red), which is defined as [23]

$$|\theta_{N,k}\rangle = \frac{1}{\sqrt{N+1}} \sum_{n=0}^{N} e^{in\theta_{N,k}} |n\rangle, \tag{6}$$

where $\theta_{N,k} = 2k\pi/(N+1)$, with $0 \le k \le N$. These probabilities are calculated according to the ideal state evolution described by Eq. (5). The results show that the optimal success probability for the two-component superposition scales as $2e^{-(N!)^{1/N}}$; when N is large, this probability is approximately $2e^{-N/e}$ and becomes impractically low since

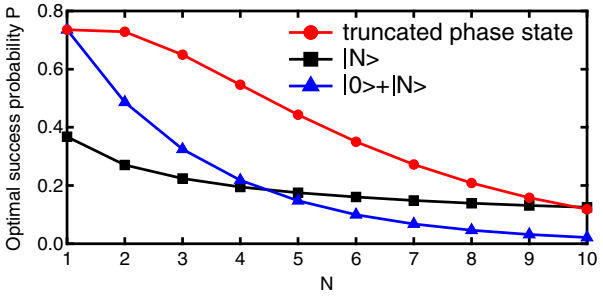

FIG. 1. State-dependent scaling of efficiency. The optimal success probabilities are plotted as functions of N for the Fock state $|N\rangle$ (black), two-component superposition $(|0\rangle + |N\rangle)/\sqrt{2}$ (blue), and truncated phase state (red) defined in Eq. (6).

the two superposed Fock state components are unlikely to occur simultaneously in any coherent state. Compared to the case of two-component superpositions, the optimal success probability for truncated phase states is larger by a factor of $(N+1)/2$ and scales more favorably because the decrease of the success probability, due to the enlarged spacing between $|0\rangle$ and $|N\rangle$, is partly compensated for by the increase of the number of superposed Fock states. The optimal success probability for producing the Fock state $|N\rangle$ is equal to the population of this Fock state in the coherent state, with an average photon number N, which drops slowly with the increase of N.

Our experiment is implemented with a superconducting circuit, where one transmon qubit is dispersively coupled to two three-dimensional cavities [20–22,24,25]. The qubit, with a transition frequency $\omega_q/2\pi = 5.345$ GHz, has an energy relaxation time $T_1 = 13.0$ μs and a pure dephasing time $T_\phi = 13.8$ μs. Cavity 1, with a frequency $\omega_s/2\pi = 8.230$ GHz and a photon lifetime $\tau_s = 80$ μs, is used for storage of the photonic state. Cavity 2, with a frequency $\omega_r/2\pi = 7.290$ GHz and a photon lifetime $\tau_r = 44$ ns, is connected to a Josephson parametric amplifier [26–29], allowing for a high-fidelity (nearly unity) and quantum nondemolition single-shot readout of the qubit state. For simplicity, the term "cavity" refers to cavity 1. The dispersive frequency shift is $\chi_{qc}/2\pi = 1.44$ MHz. The experimental apparatus and readout properties can be found in the Supplemental Material [30] and Ref. [25].

The experimental sequence is outlined in Fig. 2. The initialization of the system to $|g,0\rangle$ is realized by the postselection on the qubit's ground state and the subsequent cavity parity measurement. The initial coherent state of the cavity is achieved by the application of a microwave pulse, which produces a displacement operation $D(\alpha)$. This is followed by driving the qubit, initially in the ground state $|g\rangle$, with a pulse with $N+1$ frequency components resonant with the corresponding qubit-cavity transition frequencies, and simultaneously implementing $N+1$ conditional qubit rotations: $\prod_{n=0}^{N} R_{e_n|n}(\beta_n)$, where $R_{e_n|n}(\beta_n)$ represents the qubit rotation on the Bloch sphere by an angle β_n around the e_n direction conditional on the cavity containing n photons, with e_n being on the equatorial plane, with the azimuth angle $\phi_n + n\chi_{qc}\tau$. In order to have enough selectivity, each frequency component in the qubit pulse simply has a broad Gaussian envelope, truncated to $4\sigma = 1.44$ μs ($\sigma_f = 0.44$ MHz). Postselecting on the excited qubit state, we obtain the desired cavity state. After preparation of the desired cavity state, the qubit is disentangled with the cavity and can be used to measure the Wigner function of the cavity. Following a technique devised by Lutterbach and Davidovich [31] and demonstrated in cavity QED [32] and circuit QED [21,22,25], the Wigner quasiprobability distribution $W(\beta)$ is measured by a combination of the cavity's displacement operation $D(-\beta)$ and qubit Ramsey-type measurement, where a

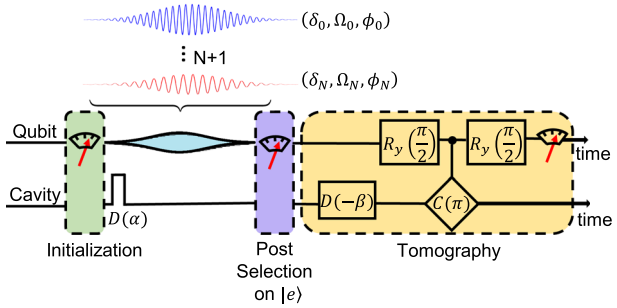

FIG. 2. Experimental sequence. The experiment starts with the application of a microwave pulse to the cavity, corresponding to a phase-space displacement operation $D(\alpha)$, which transforms the cavity from the ground state $|0\rangle$ to the coherent state $|\alpha\rangle$. Then the qubit, initially in the ground state $|g\rangle$, is driven by a classical microwave pulse comprising $N+1$ frequency components, with the nth component resonant with the qubit transition conditional on the cavity's photonic field being in the Fock state with n photons. This corresponds to simultaneous implementation of $N+1$ conditional qubit rotations on the Bloch sphere: $\prod_{n=0}^{N} R_{e_n|n}(\beta_n)$. Subsequent measurement of the qubit in the excited state $|e\rangle$ collapses the cavity to a superposition of $N+1$ Fock states, whose amplitudes are controllable by the parameters of the corresponding microwave components. A final Wigner tomography is performed to examine the produced states.

conditional cavity π phase shift $C(\pi)$ is sandwiched in between two unconditional qubit rotations $R_y(\pi/2)$.

As an example, we prepared the truncated phase states, defined by Eq. (6), with $N = 5$ to 7. Apart from the fundamental interest, such states are useful for the implementation of the quantum walk [33]. Figure 3(a) shows the ideal (left) and experimental (right) Wigner functions of the truncated phase state, with $\theta_{N,k} = 0$ and $N = 5$, while those with $N = 6$ and 7 are presented in the Supplemental Material [30]. We note that, mainly due to the decoherence of the system (see Supplemental Material [30]), the measured Wigner function $W_{\text{meas}}(\beta)$ does not satisfy the normalization condition; i.e, $f = \int W_{\text{meas}}(\beta) d^2\beta < 1$. To make the results physically meaningful, we take the reduction factor f into account and use the experimental Wigner function $W_{\text{exp}}(\beta)$, defined as $W_{\text{exp}}(\beta) = W_{\text{meas}}(\beta)/f$, to describe the quasiprobability distribution for the cavity state in phase space. The shapes of the experimental and ideal Wigner functions agree very well, implying that the quasiclassical states have been converted into the desired quantum states with high accuracy. The amplitudes α of the initial coherent states, Wigner function reduction factors f, success probabilities P, and fidelities F between the produced states and desired ones are detailed in Table I. Here, the fidelity is defined as $F = \langle\theta_{N,k}|\rho_p|\theta_{N,k}\rangle$, where ρ_p is the density operator of the produced state reconstructed by least-square regression, using a maximum likelihood estimation [34,35].

The infidelity is mainly due to the decoherence of the system and the phase deviations caused by higher-order terms that are not included in Hamiltonian of Eq. (1).

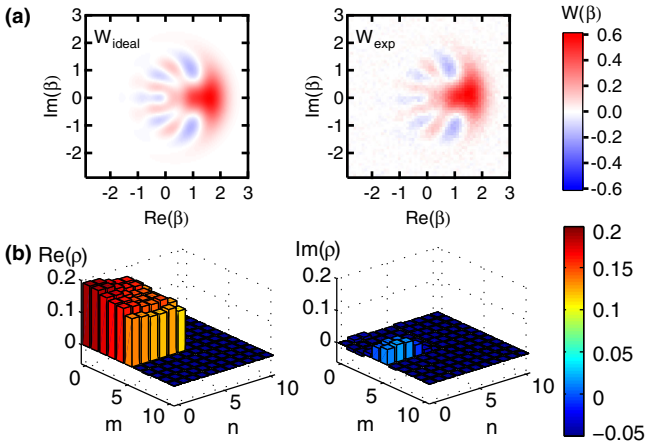

FIG. 3. Wigner tomography and density matrix reconstruction of the truncated phase state, with $\theta_{N,k} = 0$ and $N = 5$. (a) The ideal Wigner function W_{ideal} (left) and experimental Wigner function W_{exp} (right). The experimental Wigner function is defined as $W_{\text{exp}}(\beta) = W_{\text{meas}}(\beta)/f$, where $f = \int W_{\text{meas}}(\beta)d^2\beta$ is the reduction factor of the measured Wigner function $W_{\text{meas}}(\beta)$ due to the readout errors. (b) The real (left) and imaginary (right) parts of the density matrix, obtained from the experimental Wigner function W_{exp}.

However, since the desired cavity state is obtained by postselection on the qubit's excited state $|e\rangle$, its fidelity is actually very insensitive to the decoherence of the qubit. This can be explained as follows. The system evolution trajectories, involving the qubit decaying from $|e\rangle$ to $|g\rangle$, are largely excluded by projecting the qubit to $|e\rangle$, and the qubit dephasing, corresponding to a qubit frequency fluctuation, mainly produces a random phase difference between $|e\rangle$ and $|g\rangle$ but only slightly affects the cavity state correlated to $|e\rangle$ (see Supplemental Material [30] for detailed discussions). Numerical simulations show that the qubit decoherence and cavity photon decay together contribute an error of about 2% for the truncated phase state displayed in Fig. 3. To show how good the protocol can work in a system with infinite coherence, we calculate the fidelities for the truncated phase states with $N = 5$ to 7 under this ideal condition and present the results in the last row of Table I. Further numerical simulations show that in this case, the infidelity is mainly due to the photon-number-dependent phase shifts, resulting from the higher-order terms dominated by the Kerr term $-Ka^{\dagger 2}a^2/2$ and the correction to the dispersive qubit-cavity coupling $\chi'_{qc}a^{\dagger 2}a^2|e\rangle\langle e|/2$. Note that these additional phase shifts are determined by the system parameters and can be compensated for by properly setting the phases of the driving signals. The error due to the cross Kerr term between the two cavities has already been corrected in our experiment by properly setting the phase of $|\alpha\rangle$. With the wide multicomponent pulse used in our experiment, the imperfections of the conditional qubit rotations, limited by their frequency selectivity, contribute an infidelity smaller than 0.1%.

TABLE I. Amplitudes α of the initial coherent states, Wigner function reduction factors f, success probabilities P, and fidelities F of the produced truncated phase states, with $\theta_{N,k} = 0$. F_I denotes the simulated fidelities without consideration of decoherence. The uncertainties are determined by bootstrapping on the measured Wigner functions [35]. Bootstrapping allows for random sampling with replacement at each pixel point of the measured Wigner function to obtain a pool of new Wigner functions that are used to extract f and F for a statistical analysis.

N, k	5, 0	6, 0	7, 0
$\lvert\alpha\rvert$	1.63	1.74	1.85
f	0.84 ± 0.01	0.82 ± 0.01	0.80 ± 0.01
P	0.37	0.31	0.23
F	0.97 ± 0.01	0.96 ± 0.01	0.96 ± 0.01
F_I	0.99	0.99	0.99

In Fig. 3(b), we display the real (left) and imaginary (right) parts of the density matrix in Fock state representation reconstructed from the experimental Wigner function W_{exp}. The values of thus obtained matrix elements are in good agreement with the ideal results. The nonvanishing imaginary parts of the off-diagonal elements are mainly due to the imperfect setting of the relative phases of different driving microwave components. The value of the matrix element $\rho_{m,n}$ $(0 \le m, n \le N)$ slightly decreases as m and/or n increase since the decay rate is proportional to $(m + n)$.

As another example to demonstrate the ability to generate any superposition state, we produce the squeezed state

$$|\xi\rangle = \frac{1}{\sqrt{\cosh r}} \sum_{n=0}^{\infty} \frac{(-e^{i\theta}\tanh r)^n \sqrt{(2n)!}}{n!2^n} |2n\rangle, \quad (7)$$

with the squeezing parameter $\xi = re^{i\theta}$. For such a state, the fluctuation of the quadrature $X(\theta/2) = (a^\dagger e^{i\theta/2} + ae^{-i\theta/2})/2$ is reduced by a factor e^{-2r} compared to the vacuum level so that it can be used for high-precision measurement [8]. The squeezed state can be well approximated by truncating the expansion into a superposition of the first $N + 1$ Fock states, with N depending on r. We approximately produce the squeezed states for $\xi = 0.8$, $0.8i$, and -0.8, with a cutoff of $N = 8$. Figure 4 displays the

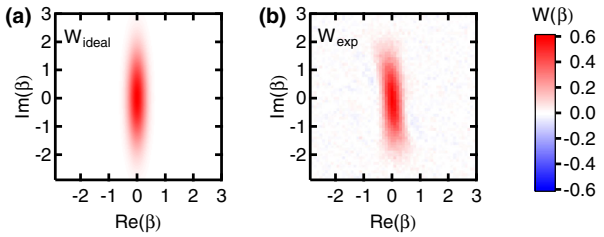

FIG. 4. Wigner tomography of the squeezed state, defined by Eq. (7), for $\xi = 0.8$. We take the cutoff in the Fock state expansion to be $N = 8$. The ideal and experimental Wigner functions W_{ideal} and W_{exp} are displayed in the left and right panels, respectively.

TABLE II. f, P, F, and $\langle[\Delta X(\theta/2)]^2\rangle$ for the produced squeezed states, with $r = 0.8$ (Fig. 4). All have an initial coherent state amplitude $|\alpha| = 1.45$.

θ	0	$\pi/2$	π
f	0.82 ± 0.01	0.84 ± 0.01	0.82 ± 0.01
P	0.15	0.14	0.14
F	0.96 ± 0.01	0.94 ± 0.01	0.96 ± 0.01
$\langle[\Delta X(\theta/2)]^2\rangle$	0.067 ± 0.001	0.070 ± 0.001	0.070 ± 0.001

ideal (left) and experimental (right) Wigner functions for the squeezed state, with $\xi = 0.8$, and those with $\xi = 0.8i$ and -0.8 are shown in Supplemental Material [30]. Table II shows the corresponding f, P, F, and $\langle[\Delta X(\theta/2)]^2\rangle$ [obtained from the Gaussian fit of the probability distribution of $X(\theta/2)$, calculated by integrating the measured Wigner function over $X(\theta/2+\pi/2)$] in the produced states. The measured $\langle[\Delta X(\theta/2)]^2\rangle \ll 1/4$, showing that the initial quasiclassical states have been converted into quantum states with strong squeezing.

In summary, we have proposed and experimentally demonstrated a new scheme to produce arbitrary superposition of Fock states for a cavity. We show that a coherent state can be conditionally converted to any desired superposition state by tailoring the probability amplitudes associated with the superposed Fock state components. This is achieved based on the experimentally convenient dispersive coupling between the cavity and the qubit. Our results open up interesting applications of nonclassical states of harmonic oscillators for the implementation of quantum information and precision measurement. Of particular interest are the demonstrated truncated phase states that are directly applicable in the quantum walk, which allows exponential speedup over classical computation for certain problems [36] and more importantly, can be used as a primitive for universal quantum computation [37].

We acknowledge Zhangqi Yin, Andrei Petrenko, Brian Vlastakis, and Haidong Yuan for helpful discussions, and thank Tanay Roy and Madhavi Chand for the help with the parametric amplifier measurements. This work was supported by the Ministry of Science and the Ministry of Education of China through its grant to Tsinghua University, the National Natural Science Foundation of China under Grant Nos. 11674060 and 11474177, the Major State Basic Research Development Program of China under Grant No. 2012CB921601, and the 1000 Youth Fellowship program in China.

*t96034@fzu.edu.cn
†lmduan@umich.edu
‡luyansun@tsinghua.edu.cn

[1] V. Bužek and P. L. Knight, Prog. Opt. **34**, 1 (1995).
[2] S. Deléglise, I. Dotsenko, C. Sayrin, J. Bernu, M. Brune, J. M. Raimond, and S. Haroche, Nature (London) **455**, 510 (2008).
[3] H. Wang, M. Hofheinz, M. Ansmann, R. C. Bialczak, E. Lucero, M. Neeley, A. D. O'Connell, D. Sank, J. Wenner, A. N. Cleland *et al.*, Phys. Rev. Lett. **101**, 240401 (2008).
[4] M. Brune, J. Bernu, C. Guerlin, S. Deléglise, C. Sayrin, S. Gleyzes, S. Kuhr, I. Dotsenko, J. M. Raimond, and S. Haroche, Phys. Rev. Lett. **101**, 240402 (2008).
[5] C. Sayrin, I. Dotsenko, X. Zhou, B. Peaudecerf, T. Rybarczyk, S. Gleyzes, P. Rouchon, M. Mirrahimi, H. Amini, M. Brune *et al.*, Nature (London) **477**, 73 (2011).
[6] X. Zhou, I. Dotsenko, B. Peaudecerf, T. Rybarczyk, C. Sayrin, S. Gleyzes, J. M. Raimond, M. Brune, and S. Haroche, Phys. Rev. Lett. **108**, 243602 (2012).
[7] K. Wódkiewicz, P. L. Knight, S. J. Buckle, and S. M. Barnett, Phys. Rev. A **35**, 2567 (1987).
[8] C. M. Caves, K. S. Thorne, R. W. P. Drever, V. D. Sandberg, and M. Zimmermann, Rev. Mod. Phys. **52**, 341 (1980).
[9] M. H. Michael, M. Silveri, R. T. Brierley, V. V. Albert, J. Salmilehto, L. Jiang, and S. M. Girvin, Phys. Rev. X **6**, 031006 (2016).
[10] K. Vogel, V. M. Akulin, and W. P. Schleich, Phys. Rev. Lett. **71**, 1816 (1993).
[11] C. K. Law and J. H. Eberly, Phys. Rev. Lett. **76**, 1055 (1996).
[12] A. Ben-Kish, B. DeMarco, V. Meyer, M. Rowe, J. Britton, W. M. Itano, B. M. Jelenković, C. Langer, D. Leibfried, T. Rosenband *et al.*, Phys. Rev. Lett. **90**, 037902 (2003).
[13] M. Hofheinz, E. M. Weig, M. Ansmann, R. C. Bialczak, E. Lucero, M. Neeley, A. D. O'Connell, H. Wang, J. M. Martinis, and A. N. Cleland, Nature (London) **454**, 310 (2008).
[14] M. Hofheinz, H. Wang, M. Ansmann, R. C. Bialczak, E. Lucero, M. Neeley, A. D. O'Connell, D. Sank, J. Wenner, J. M. Martinis *et al.*, Nature (London) **459**, 546 (2009).
[15] S. Krastanov, V. V. Albert, C. Shen, C.-L. Zou, R. W. Heeres, B. Vlastakis, R. J. Schoelkopf, and L. Jiang, Phys. Rev. A **92**, 040303 (2015).
[16] R. W. Heeres, B. Vlastakis, E. Holland, S. Krastanov, V. V. Albert, L. Frunzio, L. Jiang, and R. J. Schoelkopf, Phys. Rev. Lett. **115**, 137002 (2015).
[17] N. Khaneja, T. Reiss, C. Kehlet, T. Schulte-Herbrüggen, and S. J. Glaser, J. Magn. Reson. **172**, 296 (2005).
[18] P. de Fouquieres, S. Schirmer, S. Glaser, and I. Kuprov, J. Magn. Reson. **212**, 412 (2011).
[19] R. W. Heeres, P. Reinhold, N. Ofek, L. Frunzio, L. Jiang, M. H. Devoret, and R. J. Schoelkopf, arXiv:1608.02430.
[20] H. Paik, D. I. Schuster, L. S. Bishop, G. Kirchmair, G. Catelani, A. P. Sears, B. R. Johnson, M. J. Reagor, L. Frunzio, L. I. Glazman *et al.*, Phys. Rev. Lett. **107**, 240501 (2011).
[21] B. Vlastakis, G. Kirchmair, Z. Leghtas, S. E. Nigg, L. Frunzio, S. M. Girvin, M. Mirrahimi, M. H. Devoret, and R. J. Schoelkopf, Science **342**, 607 (2013).
[22] L. Sun, A. Petrenko, Z. Leghtas, B. Vlastakis, G. Kirchmair, K. M. Sliwa, A. Narla, M. Hatridge, S. Shankar, J. Blumoff *et al.*, Nature (London) **511**, 444 (2014).
[23] D. T. Pegg and S. M. Barnett, J. Mod. Opt. **44**, 225 (1997).
[24] A. Wallraff, D. I. Schuster, A. Blais, L. Frunzio, R.-S. Huang, J. Majer, S. Kumar, S. M. Girvin, and R. J. Schoelkopf, Nature (London) **431**, 162 (2004).

[25] K. Liu, Y. Xu, W. Wang, S.-B. Zheng, T. Roy, S. Kundu, M. Chand, A. Ranadive, R. Vijay, Y. P. Song *et al.*, Sci. Adv. **3**, e1603159 (2017).
[26] M. Hatridge, R. Vijay, D. H. Slichter, J. Clarke, and I. Siddiqi, Phys. Rev. B **83**, 134501 (2011).
[27] T. Roy, S. Kundu, M. Chand, A. M. Vadiraj, A. Ranadive, N. Nehra, M. P. Patankar, J. Aumentado, A. A. Clerk, and R. Vijay, Appl. Phys. Lett. **107**, 262601 (2015).
[28] A. Kamal, A. Marblestone, and M. H. Devoret, Phys. Rev. B **79**, 184301 (2009).
[29] K. W. Murch, S. J. Weber, C. Macklin, and I. Siddiqi, Nature (London) **502**, 211 (2013).
[30] See Supplemental Material at http://link.aps.org/supplemental/10.1103/PhysRevLett.118.223604 for a discussion of the device parameters, readout properties of the qubit state and cavity parity, details on the experimental pulse sequence, Wigner tomography, and calibration of the driving pulses, as well as a discussion of the infidelity of the produced states and the reduction of the measured Wigner functions.
[31] L. G. Lutterbach and L. Davidovich, Phys. Rev. Lett. **78**, 2547 (1997).
[32] P. Bertet, A. Auffeves, P. Maioli, S. Osnaghi, T. Meunier, M. Brune, J. M. Raimond, and S. Haroche, Phys. Rev. Lett. **89**, 200402 (2002).
[33] B. C. Sanders, S. D. Bartlett, B. Tregenna, and P. L. Knight, Phys. Rev. A **67**, 042305 (2003).
[34] J. A. Smolin, J. M. Gambetta, and G. Smith, Phys. Rev. Lett. **108**, 070502 (2012).
[35] B. Vlastakis, A. Petrenko, N. Ofek, L. Sun, Z. Leghtas, K. Sliwa, Y. Liu, M. Hatridge, J. Blumoff, L. Frunzio *et al.*, Nat. Commun. **6**, 8970 (2015).
[36] A. M. Childs, R. Cleve, E. Deotto, E. Farhi, S. Gutmann, and D. A. Spielman, in *Proc. 35th ACM Symposium on Theory of Computing* (ACM, New York, 2003), pp. 59–68.
[37] A. M. Childs, Phys. Rev. Lett. **102**, 180501 (2009).